Mechanical Systems and Signal Processing 25 (2011) 1715–1726

Contents lists available at ScienceDirect

Mechanical Systems and Signal Processing

journal homepage: www.elsevier.com/locate/jnlabr/ymssp

A new hybrid active/passive sound absorber with variable surface impedance

Benjamin Betgen *, Marie-Annick Galland

Université de Lyon, Centre Acoustique du LMFA - UMR CNRS 5509, Ecole Centrale de Lyon, 36 Avenue Guy de Collongue, 69134 Ecully Cedex, France

ARTICLE INFO

Article history:
Received 12 November 2009
Received in revised form
5 July 2010
Accepted 9 December 2010
Available online 17 December 2010

Keywords:
Acoustics
Active noise control
Absorber
Impedance

ABSTRACT

The context of the present paper is the wall treatment of flow ducts, notably aero-engine nacelle intakes and outlets. For this purpose, hybrid active/passive absorbers have been developed at the LMFA for about 15 years. A hybrid cell combines passive absorbent properties of a porous layer and active control at its rear face. Active control is mainly used to increase absorption at low frequencies by cancelling the imaginary part of the surface impedance presented by the absorber. However, the optimal impedance (i.e. the one that produces the highest noise reduction) of an absorber for flow duct applications is generally complex and frequency dependent. A new hybrid absorber intended to realise any of impedance has therefore been developed. The new cell uses one microphone on each side of a resistive cloth. Normal velocity can then be deduced by a simple pressure difference, which allows an estimation of the surface impedance of the absorber. In order to obtain an error signal related to a target impedance, the target impedance has to be reproduced in time domain. The design of a stable and causal filter is a difficult task, considering the kind of frequency response we seek. An alternative way of representing the impedance in time domain is therefore given. The new error signal is integrated into a feedback control structure. Fast convergence and good stability are observed for a wide range of target impedances. Typical optimal impedances with a positive increasing real part and a negative decreasing imaginary part have been successfully realised. Measurements in a grazing-incidence tube show that the new complex impedance absorber clearly outperforms the former active absorber.

1. Introduction

It is well known that the control of low-frequency noise by passive means requires very bulky absorbers. Active systems have therefore become an established alternative in noise control engineering. Also known as "anti-sound", the basic principle consists in superposing a secondary sound field to the undesired sound in order to create silence through destructive interference. In the case of complex sound fields, sophisticated systems involving a large number of secondary sources and error microphones are needed to create an appropriate secondary field.

An alternative to direct active control is the control of the boundary conditions of the concerned system by means of active absorbers.

* Corresponding author. Present address: VIBRATEC, 28 Chemin du Petit Bois, BP 36 - 69134 Ecully Cedex, France. Tel.: +33 4 72 86 65 42; fax: +33 4 72 86 65 66.
E-mail address: benjamin.betgen@vibratec.fr (B. Betgen).

0888-3270/$ - see front matter © 2010 Elsevier Ltd. All rights reserved.
doi:10.1016/j.ymssp.2010.12.006

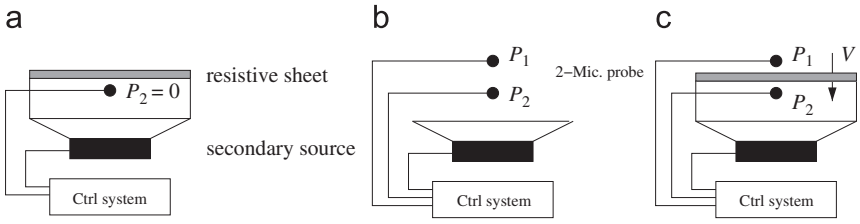

Fig. 1. Different control strategies: (a) pressure release, (b) 2-Mic. probe, and (c) impedance control.

This concept has been introduced in 1953 by Olson and May [1], who suggested to perform a pressure reduction at the rear face of a porous layer in order to enhance absorption at low frequencies. First experimental investigations were carried out by Guicking and Lorenz [2] in the 1980s. Our team developed a similar hybrid (active/passive) system and compared its performance to a direct impedance control strategy that works with a microphone and an accelerometer fixed on the membrane of the secondary source [3]. The simpler hybrid system has been privileged and was later tested for situations such as coupled vibro-acoustic cavities [4] or flow ducts [5]. Substantial and global noise reductions have been obtained with these hybrid absorbers. Fig. 1a sketches such a hybrid cell; its mode of operation can be briefly qualified as "pressure release".

A slightly different approach of controlling the boundary conditions of a system consists in detecting and controlling the reflected wave component. This technique is often called "impedance-matching" or "impedance control", however, sometimes it is also qualified as "active absorption", which may cause confusion in respect to the technique described above. Guicking and his team developed an active cell [6] that uses a two-microphone probe as outlined in Fig. 1b, capable of adjusting the reflexion coefficient to a desired value. Later they tested a 3×3 loudspeaker array in free-field conditions, intended as an active device to control the reverberation time of a room [7]. Orduña-Bustamente and Nelson [8] first used the FXLMS algorithm for such kind of active cell. Cobo et al. [9] used a two-microphone probe on the rear side of a microperforated panel in order to compare impedance matching and pressure release conditions.

Both strategies are capable of realising what is frequently considered as the perfect absorber, i.e. an absorber with a purely real surface impedance of $Z = \rho c$, with ρ the density of air and c the speed of sound in air. This impedance is also called the characteristic impedance of air Z_0. A porous layer of resistance $R = \rho c$ has to be chosen in the case of the hybrid absorber to meet this goal. However, an impedance of $Z = \rho c$ only ensures maximum absorption in the case of normal incidence. In flow ducts like ventilation ducts or turboengine nacelles, absorptive liners experience grazing incidence of sound. The impedance that is to realise here is neither purely real nor constant with frequency. A new setup (Fig. 1c), intended to realise any of impedance has therefore been developed.

The optimal impedance for a given application depends on many parameters such as geometry, source properties and flow characteristics and may be difficult to determine in practice. Section 2 deals with the determination of optimal impedance for a relatively simple setup which is also easy to implement experimentally. However, the goal of the present paper is not to provide any sensitivity analysis but to demonstrate feasibility and potential of the developed impedance control concept. Section 3 outlines the new concept and presents its practical realisation in terms of control algorithms. The used experimental installations are presented in Section 4, simulation and measurement results are exposed in Section 5.

2. The target impedance

As stated above, the optimal impedance in terms of absorption for the lined wall of a duct is complex and frequency dependent, even without flow. Note that throughout this paper, the term impedance always denotes the surface impedance of an absorber and *not* the terminal impedance of a duct. In 1953, Cremer [10] derived an analytic expression for the optimal impedance of an infinitely long absorber covering one face of a narrow rectangular duct. It is given by

$$Z_{Cremer}/Z_0 = (0.91 - 0.76i)\frac{ka}{\pi}, \tag{1}$$

where i is the imaginary unit, $k = \omega/c$ the wavenumber (with ω the angular frequency) and a the height of the duct in direction perpendicular to the liner. Eq. (1) is restricted to narrow ducts because it has been obtained on the basis of a 2D analysis. The present study is limited to the plane-wave region $ka < \pi$, so Eq. (1) can be used.

A liner of finite length evidently involves reflections at the discontinuities between rigid and lined sections. The optimal impedance of the finite liner can therefore be defined as the impedance resulting in a maximum transmission loss (TL). We choose the simplest possible setup, depicted in Fig. 2, in order to compare calculations and experiments. The computation of optimal impedance globally follows the procedure detailed in Ref. [5]: the duct is separated into three sections, an acoustically treated one and two rigid sections on either side. The sound field in the duct is expressed as a sum of modes; it has to be matched between treated and untreated sections. This is the reason, why higher order modes have to be included (15 in the present calculations), even though only plane waves are propagating in the rigid duct in the considered frequency range. The square cross-sectional duct has a side length of 66 mm. The absorber is of the same size as the duct cross-section, i.e. 1/4 of the circumference is covered by the absorber. The Ingard/Meyers impedance boundary condition is used to account

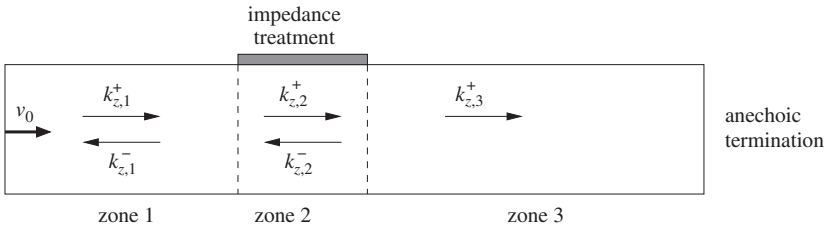

Fig. 2. Setup for the theoretical determination of optimal liner impedance.

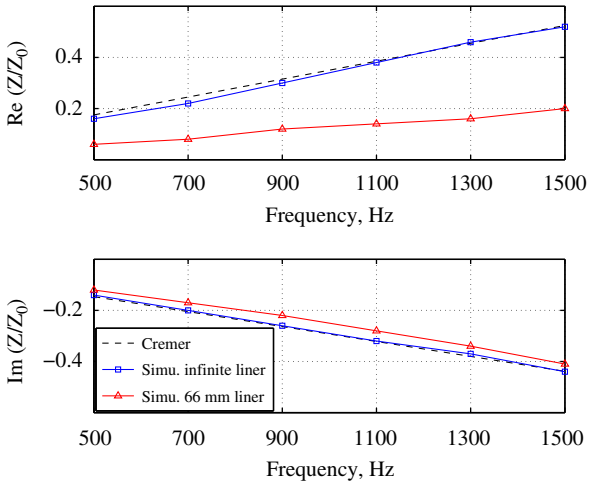

Fig. 3. Analytical determination of the optimal impedance of a (one-sided) absorber for a duct of cross-sectional area 66 mm × 66 mm. Results for an infinitely long liner and a liner of 66 mm length in comparison with the "Cremer-impedance".

for the presence of mean flow. An anechoic termination is always assumed. The axial wavenumbers $k^+_{z,2}$ and $k^-_{z,2}$ inside the treated section are computed according to Ref. [11]. Incident and transmitted power is finally determined assuming a piston-like excitation of velocity v_0 and continuity of pressure and velocity across the interfaces between the sections. Transmission loss is the logarithmised relation between incident and transmitted power. For comparison with the Cremer formula, the calculation has also been performed for an infinitely long duct, treated on one of its four sides. In this case, maximum absorption per unit length determines the optimal impedance. Fig. 3 indicates a good match between our calculation for the infinite duct and the Cremer formula, concerning resistance as well as reactance. The frequency range corresponds to non-dimensional frequencies between ka=0.6 and 1.8, i.e. well below cut-off frequency. The optimal resistance for the liner of 66 mm length is clearly decreased in respect to the infinite case. Optimal reactance does not change significantly with the length of the treatment. Only the no-flow case has been considered here, however, Section 5 includes a comparison between calculated and measured results in the presence of flow.

Remember that in the considered frequency region only plane waves are propagating in the rigid duct. When additional modes become cut-on, the optimal impedance is generally less regular and also depends on the respective modal amplitudes. The global trend of optimal impedance, however, is a positive real part that increases with frequency and a negative imaginary part that decreases with frequency. Designing an absorber that represents such kind of surface impedance is a significant progress in respect to existing absorbers. One may also object that the treated setup is a very special case and that optimal impedance will for instance be dependent on occurring reflections at the duct termination. For this reason, the consideration of insertion loss rather than transmission loss is often preferred for practical applications. Here, the setup has been chosen as "academic" as possible in order to facilitate a comparison between calculation and experiment. The aim is a demonstration of the performance of the new hybrid absorber in a given environment. However, one of the main advantages of this absorber is the possibility to realise arbitrary surface impedances that can be adopted to particular requirements.

3. Concept and realisation of impedance control

In order to better understand the new impedance control concept, the classical ("pressure release") hybrid absorber according to Fig. 1a shall quickly be reviewed. Note that the characteristic dimension of each cell has to be smaller than half the acoustic wavelength in order to assure a homogeneous pressure over the cell surface. In passive mode, the acoustic surface impedance $Z(\omega) = P_1(\omega)/V(\omega)$, with $P_1(\omega)$ the acoustic pressure in front of the absorber and $V(\omega)$ the normal acoustic

velocity, is then given by the expression $Z(\omega)=R+i\,Z_0\cot(kd)$. The real part of this impedance is controlled by the flow resistance R of the surface sheet, generally quite constant with frequency. The imaginary part is frequency dependent as it relies on the product of wavenumber k and cavity depth d. It becomes zero at frequencies $f=nc/(4d)$, with $n=1,\ 3,\ 5,\ \ldots$. As an example, a cavity depth of $d=85$ mm leads to a first purely real impedance at $f=1$ kHz. Active control can be used to drive the imaginary part to zero at low frequencies avoiding the need of a deep cavity. In fact, viscous forces in a porous material predominate over inertial ones at low frequencies and the acoustic velocity across a resistive layer can be approximated using Darcy's law. This means that acoustic velocity is proportional to the pressure difference between both sides of the resistive layer and inversely proportional to its flow resistance R, as given by

$$V(\omega)=\frac{P_1(\omega)-P_2(\omega)}{R}. \tag{2}$$

Darcy's law can be interpreted as the zeroth order approximation for acoustic propagation in a porous material. More details and a first order approximation are given in Ref. [12]. Eq. (2) can be used in order to estimate the surface impedance of the absorber as

$$Z(\omega)=\frac{P_1(\omega)}{V(\omega)}=R\frac{P_1(\omega)}{P_1(\omega)-P_2(\omega)}, \tag{3}$$

with R the known resistivity of the sheet. Obviously, the pressure release condition $P_2=0$ leads to the constant and purely real impedance $Z=R$. If the value of R is properly adjusted, high noise reduction can be obtained over a relatively broad frequency range. However, in the case of a frequency dependent optimal impedance the choice of R always represents a tradeoff between low- and high-frequency performance. The new impedance control concept overcomes this limitation.

3.1. Estimation and control of impedance

We propose to place a pair of microphones on either side of the resistive sheet (as shown in Fig. 1c) in order to measure the complex surface impedance by the use of Eq. (3). In other words, the existing hybrid cell is provided with a second microphone in front of the resistive layer. This design permits a frequency independent (in a certain frequency range) and accurate velocity measurement thanks to a significant pressure difference between the two microphones. At the same time the system remains compact, because the two microphones can be placed close to each other. In respect to a purely active impedance control concept as used in Ref. [3], the presence of a resistive layer furthermore permits passive absorption of high-frequency sound. This new strategy has been suggested by Dupont [4] for the enhancement of a hybrid absorber intended to reduce sound radiation emitted by an enclosure. It is developed in detail in Ref. [13] and adopted to the flow duct case in Ref. [14].

Considering again Eq. (3), it becomes clear that impedances $Z\neq R$ can be realised by adequately rearranging P_1 and P_2 instead of simply cancelling P_2. The error signal that is to minimise in order to realise a given target impedance Z_t becomes

$$E(\omega)=Z_t(\omega)[P_1(\omega)-P_2(\omega)]-RP_1(\omega). \tag{4}$$

Just as the classical hybrid absorber, the new absorber is intended to operate in active mode at low frequencies and in passive mode at higher frequencies. This is a considerable advantage in respect to purely active strategies that only operate at low frequencies.

3.2. Representation of the target impedance in time domain

ANC has experienced significant improvements and industrial applications with the introduction of digital filters. Autoadaptive digital filters for example are able to track changes of the primary excitation and of environmental conditions. Digital filters also permit to take into account the frequency responses of control sensors and actuators. The use of an autoadaptive digital filter as controller therefore seems a natural choice, however, it requires the design of the entire control system as a real time application. Inverse Fourier transform of the variables in Eq. (4) leads to

$$\varepsilon(t)=[z_t*(p_1-p_2)](t)-Rp_1(t) \tag{5}$$

in continuous time domain, with z_t the impulse response of the target impedance. The $*$ symbol stands for a convolution. In discrete time domain, Eq. (5) reads

$$\varepsilon(n)=[h_z*(p_1-p_2)](n)-Rp_1(n), \tag{6}$$

where h_z corresponds to the discretisation of the impulse response z_t. Here we deal with a discrete convolution. The challenge for the use of this error signal is the identification of a stable and causal filter h_z representing the target impedance in time-domain. Considering the kind of response we seek, this can be a difficult task. Some types of frequency responses, however, can be obtained easily. A real and constant target impedance $Z_t(\omega)=Z_r$ for example does not pose any problem as it is valid in frequency as well as in time domain. Additionally, the convolution reduces to a simple product and Eq. (6) becomes

$$\varepsilon(n)=Z_r[p_1-p_2](n)-Rp_1(n). \tag{7}$$

Let us now consider the realisation of a purely imaginary impedance $Z_t(\omega)=i\omega\alpha$ which is proportional to frequency. With a negative proportionality factor α, this represents the imaginary part of the Cremer impedance for instance. In fact, a multiplication

by $i\omega$ in frequency domain $Y(\omega) = i\omega X(\omega)$ corresponds to a derivation in time domain $y(t) = x'(t)$. In discrete time domain, the derivation can be approximated by $y(n) = F_s(x(n) - x(n-1))$, where F_s is the sampling frequency.

Combining gain and derivator, we can also obtain a target impedance with a constant real part and a negative imaginary part, decreasing with frequency. For cases where the real part of the optimal impedance is relatively constant with frequency (see Fig. 3), this may be sufficient. The present paper deals with the development of a feedback controller for tonal noise, that will be detailed in Section 3.3. In this case, the value of Z_r can of course be chosen to the respective optimal value.

The proposed impedance control can also be realised using a feedforward control scheme when a signal correlated to the disturbance is available. Broadband control is then feasible. If a frequency dependent real part is to be achieved, a filter representing the desired frequency response has to be identified. This can be a challenge in itself, however, in the present paper we concentrate on control of tonal noise by means of a feedback controller.

3.3. Control algorithm

In order to obtain an autonomous smart material that is independent of any reference signal, a feedback structure has been chosen. The basic idea of a digital feedback controller is to estimate the primary noise at the error sensor and to use it as the reference signal for the adaptive filter. The use of an internal model control (IMC, Morari et al.[15]) feedback configuration enables feedforward control through the filtered-x least mean squares (FXLMS) algorithm. The FXLMS algorithm itself is a modification of the standard LMS algorithm employed in feedforward control, to meet the need to include the effects of the unknown acoustic secondary-path transfer function S between the secondary source and the error sensor by modelling it with an additional finite-impulse-response (FIR) filter $\hat{S}$. This algorithm is consequently widely used in ANC applications. The IMC architecture is based on a reference signal regeneration technique whereby the secondary signal is filtered by $\hat{S}$ and then subtracted from the error signal to generate an estimation of the primary noise. This reference signal is then used as input by the ANC filter. A complete adaptive feedback system using the IMC-FXLMS algorithm is illustrated in Fig. 4 for the classical pressure cancellation case. Note that the transfer function S, which is in the physical domain, is represented as an ellipsoid, while filters in the digital domain, as the adaptive filter W, are represented by rectangles. Furthermore, $d(n)$ is the primary disturbance, $\hat{x}(n)$ the estimated reference and $y(n)$ the control output.

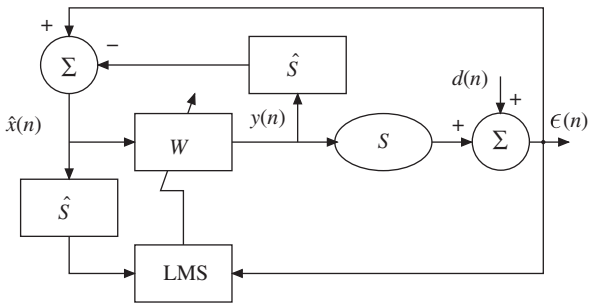

Fig. 4. IMC-FXLMS architecture.

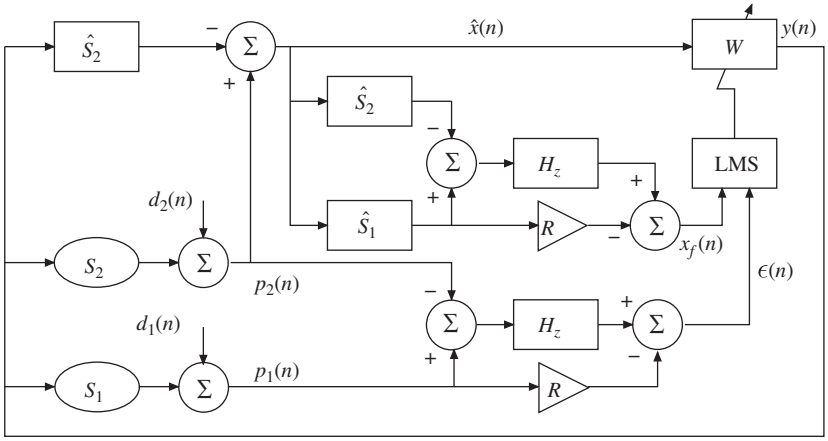

Fig. 5. Feedback IMC-FXLMS impedance control architecture.

The error signal given by Eq. (6) will be included in this IMC-FXLMS algorithm. At the moment, one single hybrid cell is considered, but control of multiple cells in parallel as proposed by Mazeaud [16] should also be feasible. Fig. 5 represents the complete scheme of the proposed feedback impedance control. Now, two secondary-path transfer functions S_1 and S_2 have to be represented as filters $\hat{S_1}$ and $\hat{S_2}$. R is the resistance of the resistive layer, a simple gain. It is not detailed in this block diagram, whether the representation of the target impedance H_z is realised as a filter or a combination of gain and derivator.

The IMC-loop that delivers an estimation of the reference signal $\hat{x}$ is obtained using microphone 2. The control output *y(n)* passes through the secondary-path filters S_1 and S_2 to contribute to the microphone signals $p_1(n)$ and $p_2(n)$ together with the primary disturbances $d_1(n)$ and $d_2(n)$. The error signal $\varepsilon(n)$ is calculated by the use of these two microphone signals. The filtered reference $x_f(n)$ is obtained by passing the estimation of the reference $\hat{x}(n)$ through the secondary-path filters and a subsequent treatment similar to the one for the error signal.

As suggested above, the real part of the target impedance Z_r can be adjusted to the respective optimal value when tonal noise is controlled. This is actually done automatically by the use of a frequency detection system. Mazeaud [16] proposed a parallelised algorithm able to control several hybrid cells without excessively increasing the computational cost. A bandpass filtering centred around the frequencies of interest and applied on the synthesised references was necessary in order to guarantee stability. An adaptive notch filter was used as a frequency tracking system that permitted to adapt the bandpass filters and as a consequence to control changing tones. The same system is used here to adapt the target resistance Z_r.

3.4. The optimal control filter

The optimal control filter W^{opt} is defined as the one that drives the error signal given by Eq. (4) to zero. We deal with a digital system here, so W^{opt} will be written in z-domain and Eq. (4) becomes

$$Z_t(z)[P_1(z)-P_2(z)]-RP_1(z)=0. \tag{8}$$

Alternatively, Eq. (8) can directly be deduced from the scheme in Fig. 5. In the following, we assume perfect identification of the secondary paths, i.e. $\hat{S_1}(z)=S_1(z)$ and $\hat{S_2}(z)=S_2(z)$, this implies that the estimation of the reference is perfect, i.e. $\hat{X}(z)=X(z)$.

Acoustic pressure at the two microphone locations is the sum of primary disturbance and control action, in z-domain this writes

$$P_1(z)=D_1(z)+X(z)W^{opt}(z)S_1(z)$$

and

$$P_2(z)=D_2(z)+X(z)W^{opt}(z)S_2(z).$$

As the IMC-loop is realised using the signal of microphone 2, it follows that $D_2(z)=X(z)$. Now, the optimal filter can be written as

$$W^{opt}(z)=-\frac{(Z_t(z)-R)D_1(z)/D_2(z)-Z_t(z)}{(Z_t(z)-R)S_1(z)-Z_t(z)S_2(z)}. \tag{9}$$

For a target impedance that equals the resistance of the resistive layer ($Z_t=R$), Eq. (9) reduces to

$$W^{opt}(z)=-\frac{1}{S_2(z)}. \tag{10}$$

Note that in this case the optimal control filter only depends on the secondary path. In the general case of Eq. (9), however, it depends on both primary and secondary paths and hence strongly on the environment of the hybrid cell. It is therefore difficult to draw conclusions about the nature of this optimal control filter. In any case, it is a noncausal filter, just as Eq. (10). As a consequence, it cannot be obtained over a broad frequency band but only at discrete frequencies. An example of an optimal control filter calculated with measured transfer functions and its realisation with a feedback controller can be found in Section 5.1.

4. Experimental setups

4.1. The hybrid absorber

The first version of a new hybrid cell was designed for the no-flow case. It is made of a feltmetal sheet with a measured resistivity of $R=220$ Ns/m^3 backed by a cavity of approximately 20 mm depth. As the rear side of the cavity is formed by a loudspeaker (Visaton SC 8 N) as secondary source, its depth is not completely homogeneous. Previous versions of hybrid absorbers had been built by using piezoelectric actuators, which offers the advantage of a more compact system. In this early stage of the study we instead prefer the simplest possible system. The front face surface of the cell is 66 mm $\times$ 66 mm. A Panasonic WM-64 electret condenser microphone is fixed on either side of the feltmetal sheet.

A second version has been designed using a wiremesh cloth glued on a perforated panel. The resistivity of this assembly is very similar to the feltmetal sheet. An additional perforated panel has been mounted at 10 mm distance in front of the resistive layer in order to protect the front face microphone from grazing flow. With an open area ratio of 25%, this panel represents a very low acoustic resistance. Due to very fine (0.54 mm) perforations it assures a good protection from grazing flow. This assembly is shown in the right hand side of Fig. 8 in conjunction with the grazing-incidence tube.

4.2. The standing wave tube

The impedance realised by the hybrid cell is measured in a standing wave tube of cross-section 55 mm × 55 mm and L=1.03 m length using the two-microphone method. The setup is sketched in Fig. 6. Signal generation and acquisition are performed using a Siglab® system. The surface impedance is computed with Matlab® software for a frequency range from 300 Hz to 1.5 kHz.

4.3. The grazing-incidence tube

The grazing-incidence tube MATISSE, displayed in Figs. 7 and 8, consists in a square cross-sectional duct (66 mm × 66 mm) whose length is approximately 3.20 m. The anechoic downstream termination is achieved thanks to an exponential outlet. The hybrid liner is applied on the upper wall of the test section. Three flush-mounted microphones (Brüel & Kjær® 1/4"), thereof two located upstream and one located downstream the test region, measure the differential pressure. The transfer functions between the primary source and the three microphones are recorded with a National Instruments® 9234 signal acquisition module on a cDAQ 9172 chassis. LabView® software is used to compute transmission loss. The studied frequency range from 500 Hz to 1.5 kHz

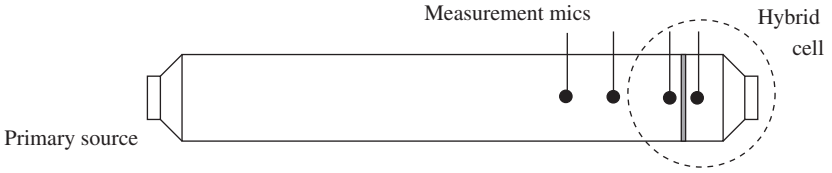

Fig. 6. Standing wave tube for impedance measurements.

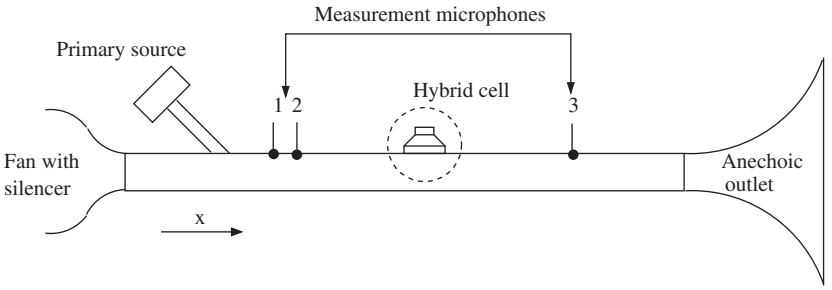

Fig. 7. Grazing-incidence tube for transmission loss measurements.

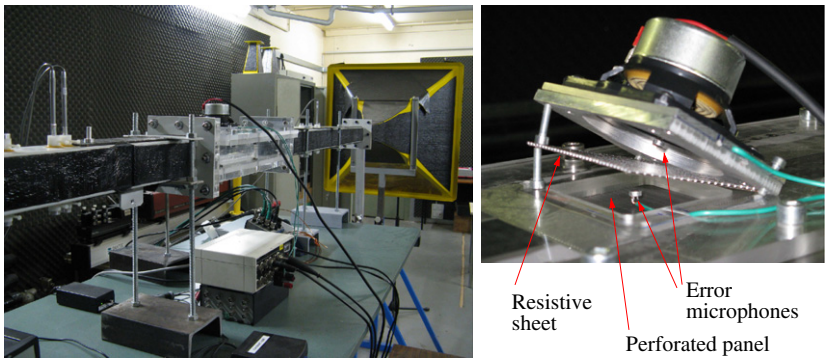

Fig. 8. Grazing-incidence tube MATISSE with the hybrid cell mounted on the test section and detail of the hybrid cell.

remains in the plane-wave region (cut-off frequency is at 2575 Hz). Even though the absorber is most probably effective at even lower frequencies, the test bench is not well adapted for measurements below 500 Hz. See also Ref. [5] for a more detailed description of the MATISSE test bench.

5. Results

5.1. Simulation results

Primary and secondary paths of a hybrid cell mounted on the MATISSE test bench have been measured. These are used for the computation of the optimal control filter (Eq. (9)) and for the control simulations that are presented in this section. A feedback control scheme corresponding to the one outlined in Fig. 5 has been built with Simulink® software. The sampling frequency is set to 10 kHz, the excitation frequency is of 500 Hz. The controller is realised with a filter of 20 coefficients. Fig. 9 displays the optimal control filter for a frequency range from 0 to 1.5 kHz in amplitude and phase. The positive slope of the phase indicates a noncausal filter. This is the reason why it cannot be obtained in broadband, but only at discrete frequencies. We note that the adaptive filter effectively converges towards the optimal solution at the given frequency. The optimal solution could also be achieved using less filter taps but the bandpass effect would be less pronounced then. The target impedance is of $Z_t/R=1-i$ here; different target impedances do not substantially change the shape of the curves.

5.2. Experimental results

For experimental validation, the feedback control scheme developed in Simulink® is executed in real time on a dSpace® DSP-board. Low-pass filter for anti-aliasing on the input side and smoothing on the output side of the DSP are set to 2 kHz.

5.2.1. Convergence

In order to visualise the convergence process, the measured time signals of both error microphones and the control output are given. Again, a pure tone of 500 Hz is the primary disturbance, and the target impedance is of $Z_t/R=1-i$. The upper part of Fig. 10 shows the convergence process, control is switched on at 5 ms. We observe that the algorithm converges in about 30 or 40 ms, however, the chosen convergence coefficient is not at its possible maximum. The lower part shows a zoom on the same signals 1 s later. Clearly, the control action does not minimise the microphone signals but rearranges them in amplitude and phase in a way to obtain the desired surface impedance.

5.2.2. Impedance measurements in the standing wave tube

The surface impedance realised by the hybrid cell is measured using the tube described in Section 4.2. The hybrid cell without protecting panel is considered here, so the reference section is the front face of the resistive layer. A frequency range from 300 Hz to 1.5 kHz is scanned, frequency is detected automatically. Fig. 11 shows that the "Cremer-impedance" can globally be well reproduced. However, the proportionality factor α that defines the slope of the target reactance had to be modified to fit the displayed imaginary part of the "Cremer-impedance". In fact, Eq. (3) represents a low-frequency approximation that holds up to approximately 500 Hz for the used feltmetal screen. At higher frequencies, a reactance is introduced mainly due to the tortuosity of the material. This reactance is proportional to frequency, therefore it can be accounted for by adapting the proportionality factor α.

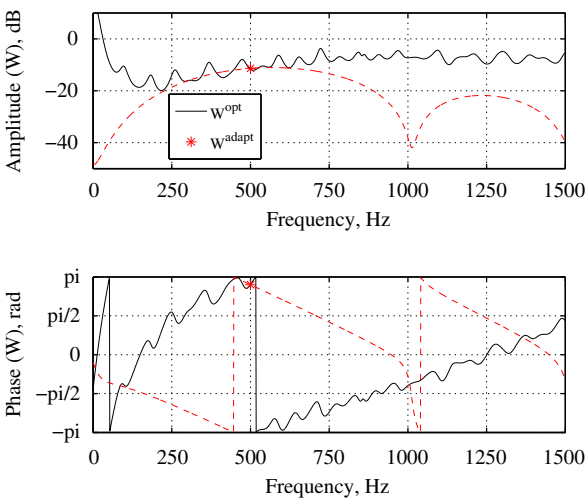

Fig. 9. Optimal control filter for a target impedance of $Z_t/R=1-i$ and its realisation with a feedback controller at 500 Hz.

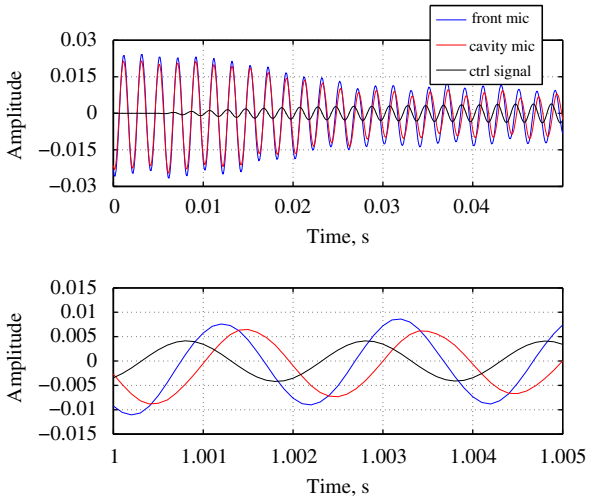

Fig. 10. Time signals of error microphones and control output.

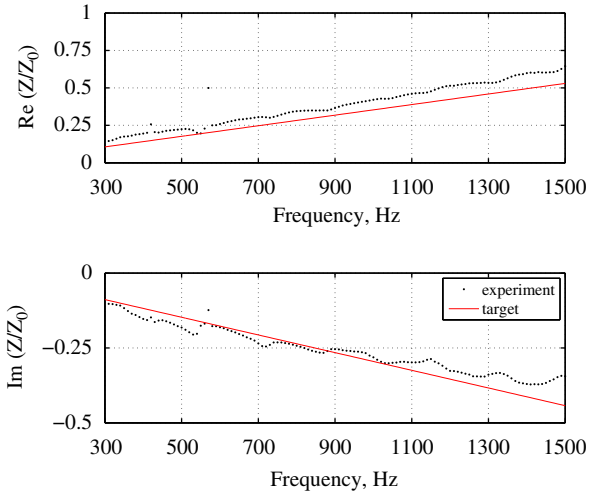

Fig. 11. Experimental realisation of the Cremer optimal impedance.

Manifestly, the control system does not well converge at 420 and 570 Hz due to occurring resonances. These frequencies correspond well to the open tube resonances of $5c/(4L)$=413 Hz and $7c/(4L)$=578 Hz. In fact, the resonance at $3c/(4L)$=248 Hz even led to a complete divergence of the control system; this is the reason why the scan starts at 300 Hz. Note that these resonances do not occur when targeting impedances closer to ρc, i.e. impedances resulting in higher absorption. However, very low impedances can be realised, but the measurement in the standing wave tube is then limited to discrete frequencies avoiding the tube resonances.

5.2.3. Transmission loss measurements in the grazing-incidence tube

The first presented measurement campaign deals with impedance values of the "Cremer-type". Different impedance functions, as given in Fig. 12a are tested. The modification of the imaginary part slope, as determined in Section 5.2.2 is used. All results presented here are obtained with one single hybrid cell of size 66 mm × 66 mm. The measured transmission loss (TL) for the no-flow case is given in Fig. 12b. Passive mode and pressure release case ("p_2=0") are given in addition to the impedance control cases that use the target impedances displayed in Fig. 12a. Passive absorption is low, but the presence of the loudspeaker slightly increases the TL in respect to a completely rigid cavity. In agreement with previous studies, pressure cancellation at the rear face of the porous layer increases the TL at low frequencies. Significantly higher TL, however, could be realised with the new impedance control. Impedance no. 1 is the Cremer impedance, i.e. the optimal impedance for an infinitely long absorber. Impedance no. 2 is an approximation of the impedance determined to be the optimal one for a liner of 66 mm length (see Section 2), i.e. the present setup. Tests with different target impedances showed that even higher TL can be obtained with slightly different settings. One such result has been computed (impedance no. 3, having a decreased resistance

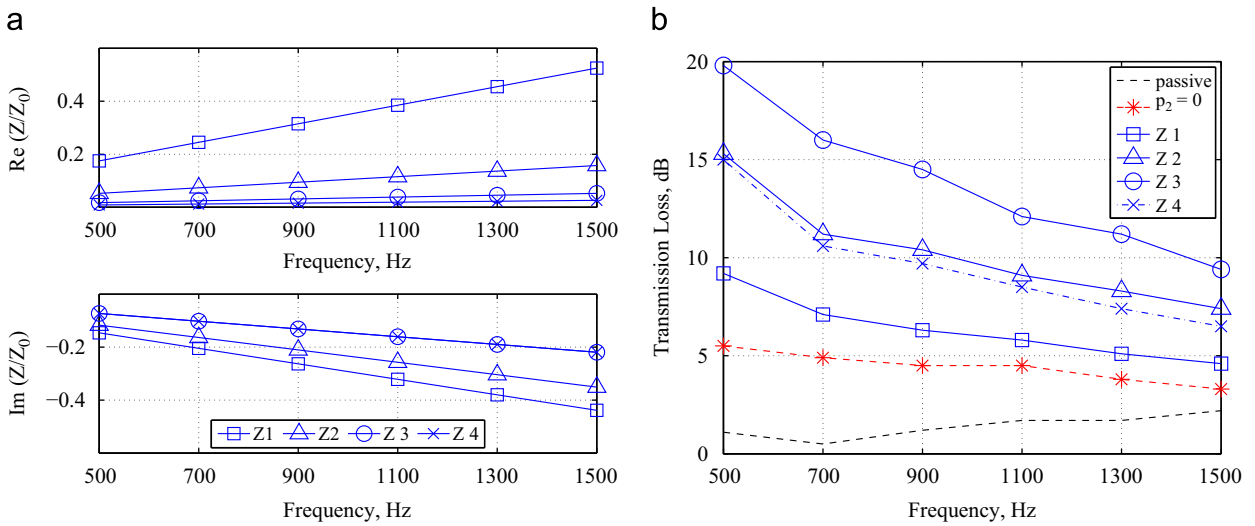

Fig. 12. Measurement of transmission loss through the treated section of the MATISSE test bench; the impedance treatment is of size 66 mm × 66 mm: (a) realised impedances and (b) corresponding transmission loss.

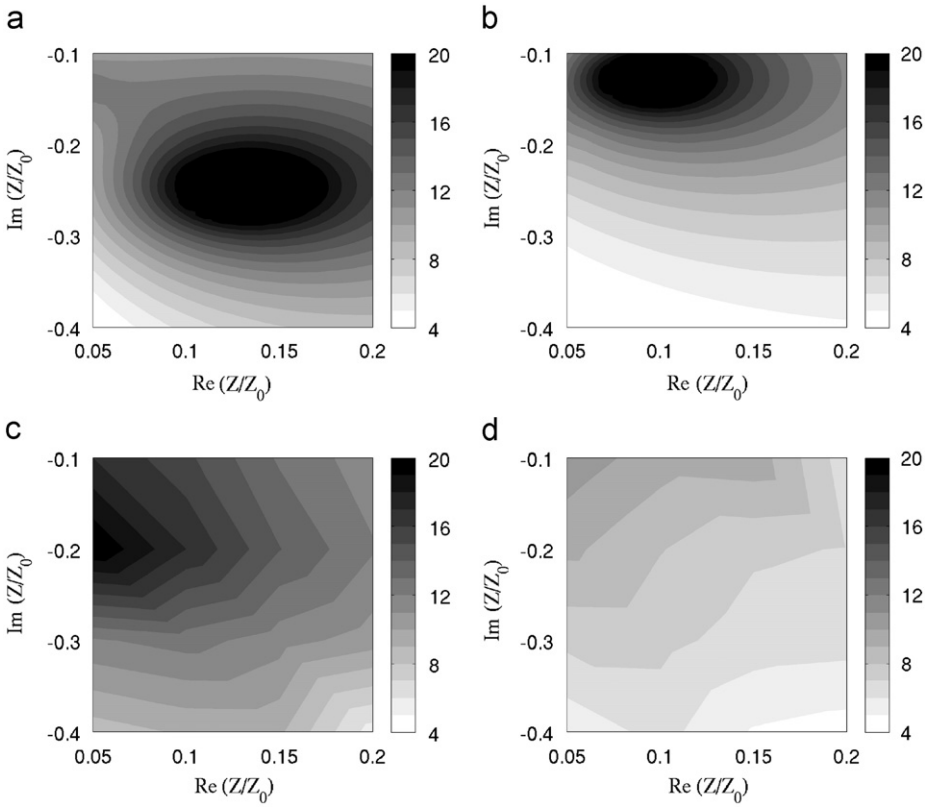

Fig. 13. Comparison of theoretically and experimentally determined transmission loss at 1 kHz: (a) calculation $M=0$, (b) calculation $M=0.1$, (c) experiment $M=0$, and (d) experiment $M=0.1$.

in respect to impedance no. 2), however, it does not necessarily represent the exact optimum. Considering these results, one could think that the optimum is actually at $Re(Z)=0$; this is in fact not the case. The last curve (impedance no. 4) shows that the TL falls anew for very low resistances. Still, the best performance of this short absorber has been found for quite low resistances, i.e. reflection contributes considerably to the obtained transmission loss.

There may be several reasons for the fact that the best performance has not been found at the calculated optimum. First of it all, there is a given uncertainty concerning the realised impedance, even though the imaginary part is corrected to account for the reactance introduced by the feltmetal sheet. Another fact finally amplifies the error: the TL varies quickly nearby the optimal impedance value, small imperfections therefore have a strong impact. Finally, the reliability of the theoretical determination of optimal impedance will also have to be checked, particularly in the case of such short treatments.

A second measurement campaign deals with the experimental determination of the optimal impedance at 1 kHz, without and with grazing flow. The hybrid cell with a protecting perforated panel is used. A bandpass filtering centred around 1 kHz and applied on the synthesised references ensures convergence of the algorithm despite high levels of flow induced noise. In order to provide accurate reproduction of the targeted impedances, the correct settings have now been determined using the standing wave tube. As impedance is measured at the front face of the perforated panel, these measurements permit at the same time to compensate for the impedance change due to this panel. An experimental scan (4×4 values) of the complex impedance plane has been performed. The obtained transmission loss is given in Fig. 13c without flow and in Fig. 13d with grazing flow of bulk Mach number 0.1 (i.e. an average flow of 34 m/s).[1] Figs. 13a and b show the theoretically determined transmission loss. The computation, discussed in Section 2, assumes a uniform flow of Mach number 0.1 using the Ingard/Meyers boundary condition [17].

All figures are plotted with the same dynamics (4–20 dB) even though the theoretically determined maximum TL is of about 40 dB for the case without as well as with flow. However, these maximum values are reached only for an extremely small impedance range and are therefore of little practical interest. Again, one observes that the highest TL are measured at lower resistances than predicted. The agreement between the imaginary parts is slightly better. The presence of flow shifts the optimal impedance towards smaller reactances, a fact that can be observed theoretically as well as experimentally. An important discrepancy, however, consists in the obtained level of TL. The calculation predicts a shift of the optimal impedance without any considerable change in the maximally achievable TL. By contrast, the measured TL decreases quite significantly, notably in those impedance regions that give rise to high TL without flow. Again, the calculations will have to be reviewed, especially concerning the assumption of uniform flow.

6. Conclusions

The conducted experiments show that the new hybrid cell can yield typical optimal impedance functions for flow duct applications. Transmission loss values up to 20 dB have been obtained with one single hybrid cell whose surface equals the cross-sectional area of the grazing-incidence tube. In order to obtain a similar performance with the former hybrid absorber, four cells instead of one had been needed. In addition, the former hybrid absorber only reached this performance when a layer of low resistance—less suited to high-frequency absorption—is chosen. It becomes clear that the new system offers a double advantage: on the one hand, optimal impedance can be well reproduced in the low-frequency region. On the other hand, a porous layer of higher resistance can be used, which is favourable to high-frequency absorption. Performance is therefore improved in active as well as in passive mode.

It must be pointed out that transmission loss is only one possible criterion allowing to assess the performance of the hybrid absorber. Absorption would be an alternative parameter to compare pressure release and impedance control modes. It can actually be measured using the same experimental setup by performing a power balance. However, the goal of the present study was to show the feasibility of a new impedance control concept. In a given application, the absorber could be tuned in a way to minimise any desired cost function.

The principal inconvenience of the proposed system is the lack of precision in the reproduction of a target impedance in the higher frequency region. The used resistive layers (a wiremesh and a feltmetal sheet) introduce an imaginary part due to the tortuosity of the material, which has to be accounted for at frequencies above 500 Hz. During the present study, the correct settings of the control system were therefore determined with the aid of impedance measurements in a standing wave tube. In the future, a method similar to the *in situ* impedance measurement method [18] may be used in order to compensate for this error automatically.

A perforated panel has been successfully used in order to protect the front face microphone from grazing flow. The new hybrid absorber permitted an experimental scan of the complex impedance plane. In contrast to theoretical predictions, an important decrease in performance has been observed in presence of grazing flow. Finer simulations, considering in particular more realistic flow profiles, should be carried out in order to determine the origin of this effect. Also the assumption of constant resistance of the front face panel in presence of flow should be verified.

Despite the outlined difficulties with high-speed grazing flow, the proposed hybrid absorber may be used in lower speed applications such as ventilation ducts. In fact, when higher order modes or complex geometries are involved, this system could be an interesting alternative to direct active control. Finally, the possibility of realising arbitrary complex surface impedances is interesting for different laboratory tests that need a control of impedance boundary conditions. One might think of impedance eduction techniques [19] that are validated for a quite narrow range of passively realised impedances at present. In this context, there is an important potential for active control techniques that is barely exploited today.

[1] In the MATISSE test bench, an average flow of 34 m/s corresponds to a maximal speed of about 50 m/s in the centre of the tube.

References

[1] H.F. Olson, E.G. May, Electronic sound absorber, Journal of the Acoustical Society of America 25 (6) (1953) 1130–1136.
[2] D. Guicking, E. Lorenz, An active sound absorber with porous plate, Journal of Vibration, Acoustics, Stress and Reliability in Design 106 (1984) 389–392.
[3] M. Furstoss, D. Thenail, M.-A. Galland, Surface impedance control for sound absorption: direct and hybrid passive/active strategies, Journal of Sound and Vibration 203 (2) (1997) 219–236.
[4] J.-B. Dupont, M.-A. Galland, Active absorption to reduce the noise transmitted out of an enclosure, Applied Acoustics 70 (1) (2009) 142–152.
[5] N. Sellen, M. Cuesta, M.-A. Galland, Noise reduction in a flow duct: implementation of a hybrid passive/active solution, Journal of Sound and Vibration 297 (2006) 492–511.
[6] K. Karcher, D. Guicking, Active impedance control for one-dimensional sound, Journal of Vibration, Acoustics, Stress, and Reliability in Design 106 (1984) 393–396.
[7] D. Guicking, K. Karcher, M. Rollwage, Coherent active methods for applications in room acoustics, Journal of the Acoustical Society of America 78 (4) (1985).
[8] F. Orduña Bustamente, P.A. Nelson, An adaptive controller for the active absorption of sound, Journal of the Acoustical Society of America 91 (5) (1992).
[9] P. Cobo, J. Pfretzschner, M. Cuesta, D.K. Anthony, Hybrid passive-active absorption using microperforated panels, Journal of the Acoustical Society of America 116 (4) (2004) 2118–2125.
[10] L. Cremer, Theorie der Luftschall-Daempfung im Rechteckkanal mit schluckender Wand und das sich dabei ergebende hoechste Daempfungsmass, Acustica 3 (1953) 249–263.
[11] S.W. Rienstra, A classification of duct modes based on surface waves, Wave Motion 37 (2003).
[12] M.-A. Galland, B. Mazeaud, N. Sellen, Hybrid passive/active absorbers for flow ducts, Applied Acoustics 66 (2005) 691–708.
[13] J.-B. Dupont, M.-A. Galland, A new hybrid passive/active cell to realize a complex impedance boundary condition, Journal of the Acoustical Society of America 123 (5) (2008) 3572.
[14] B. Betgen, M.-A. Galland, Active Control of complex surface impedance, in: 15th AIAA/CEAS Aeroacoustics Conference, Hyatt Regency Miami, 11–13 May 2009.
[15] M. Morari, E. Zafiriou, Robust Process Control, Prentice-Hall, Englewood Cliffs, NJ, 1989.
[16] B. Mazeaud, M.-A. Galland, A multi-channel feedback algorithm for the development of active liners to reduce noise in flow duct applications, Mechanical Systems and Signal Processing 21 (7) (2007) 2880–2899.
[17] M.K. Myers, On the acoustic boundary condition in the presence of flow, Journal of Sound and Vibration 71 (3) (1980) 429–434.
[18] P.D. Dean, An in situ method of wall acoustic impedance measurement in flow ducts, Journal of Sound Vibration 34 (1) (1974) 97–130.
[19] M.G. Jones, T.L. Parrott, W.R. Watson, Comparison of acoustic impedance eduction techniques for locally-reacting liners, in: 9th AIAA/CEAS Aeroacoustics Conference, Hilton Head, South Carolina, AIAA Paper 2003-3306, 12–14 May 2003.